Parallel phase modulation scheme for interferometric gravitational-wave detectors

M. T. Hartman,[1,*] **V. Quetschke,**[2] **D. B. Tanner,**[1] **D. H. Reitze,**[1,3] **and G. Mueller**[1]

[1]*Department of Physics, University of Florida,
P O Box 118440, Gainesville, Florida 32611, USA*
[2]*Department of Physics and Astronomy, University of Texas at Brownsville,
80 Fort Brown, Brownsville, Texas 78520, USA*
[3]*LIGO Laboratory, California Institute of Technology,
MS 100-36, Pasadena, California 91125, USA*

[*]*hartman@phys.ufl.edu*

Abstract: Advanced LIGO (aLIGO) requires multiple frequency sidebands to disentangle all of the main interferometer's length signals. This paper presents the results of a risk reduction experiment to produce two sets of frequency sidebands in parallel, avoiding mixed 'sidebands on sidebands'. Two phase modulation frequencies are applied to separate Electro-Optic Modulators (EOMs), with one EOM in each of the two arms of a Mach-Zehnder interferometer. In this system the Mach-Zehnder's arm lengths are stabilized to reduce relative intensity noise in the recombined carrier beam by feeding a corrective control signal back to the Rubidium Titanyl Phosphate (RTP) EOM crystals to drive the optical path length difference to zero. This setup's use of the RTP crystals as length actuators provides enough bandwidth in the feedback to meet arm length stability requirements for aLIGO.

References and links

1. B. Abbot and the LIGO Scientific Collaboration, "LIGO: the laser interferometer gravitational-wave observatory," Rep. Prog. Phys. **72**, 076901 (2009).
2. G. M. Harry for the LIGO Scientific Collaboration, "Advanced LIGO: the next generation of gravitational wave detectors," Class. Quantum Grav. **27**, 084006 (2010).
3. B. Abbot and the LIGO Scientific Collaboration, "First upper limits from LIGO on gravitational wave bursts," Phys. Rev. D **69**, 102001 (2004).
4. B. Abbot and the LIGO Scientific Collaboration and the Virgo Collaboration, "An upper limit on the stochastic gravitational-wave background of cosmological origin," Nature **460**, 990–994 (2009).
5. J. Abadie and the LIGO Scientific Collaboration and the Virgo Collaboration, "Directional limits on persistent gravitational waves using LIGO S5 science data," Phys. Rev. Lett. **107**, 271102 (2011).
6. J. Aasi and the LIGO Scientific Collaboration, "Prospects for localization of gravitational wave transients by the advanced LIGO and advanced virgo observatories," Living Rev. Relat., in press. (arXiv:1304.0670 [gr-qc], LIGO-P1200087).
7. H. Grote, A. Freise, M. Malec, G. Heinzel, B. Willke, H. Lck, K. A. Strain, J. Hough, K. Danzmann, "Dual recycling for GEO 600," Class. Quantum Grav. **21**, S473 (2004).
8. E. D. Black, "An introduction to pound–drever–hall laser frequency stabilization," Am J Phys **69**, 79–87 (2001).

9. K. A. Strain, G. Mueller, T. Delker, D. H. Reitze, D. B. Tanner, J. E. Mason, P. A. Willems, D. A. Shaddock, M. B. Gray, C. Mow-Lowry, D. E. McClelland, "Length sensing in advanced LIGO," Appl. Opt. **42**, 1244–1256 (2003).

10. R. Abbott, R. Adhikari, S. Ballmer, L. Barsotti, M. Evans, P. Fritschel, V. Frolov, G. Mueller, B. Slagmolen, and S. Waldman, "Advanced LIGO length sensing and control final design," (2010). LIGO-T1000298-T.

11. B. W. Barr, O. Miyakawa, S. Kawamura, A. J. Weinstein, R. Ward, S. Vass, and K. A. Strain, "Control sideband generation for dual-recycled laser interferometric gravitational wave detectors," Class. Quantum Grav. **23**, 5661 (2006).

12. O. Miyakawa, S. Kawamura, B. Abbott, R. Bork, P. Fritschel, L. Goggin, J. Heefner, A. Ivanov, F. Kawazoe, C. Mow-Lowry, A. Ourjoumtsev, S. Sakata, M. Smith, K. A. Strain, R. Taylor, D. Ugolini, S. Vass, R. Ward, A. Weinstein, "Sensing and control of the advanced LIGO optical configuration," SPIE 5500, Gravitational Wave and Partical Astrophysics pp. 92–104 (2004).

13. M. Arain, A. Lucianetti, R. Martin, G. Mueller, V. Quetschke, D. Reitze, D. Tanner, and W. Wu, "AdvLIGO phase modulator assembly document," (2009). LIGO-T0900475-v2.

14. S. Wise, "Sensitivity enhancement in future interferometric gravitational wave detectors," Ph.D. thesis, The University of Florida (2006).

15. S. Kawamura and O. Miyakawa, "Effect of mach zehnder residual displacement noise on the 40m detuned rse interferometer," (2004). LIGO-T040166.

16. K. L. Dooley, M. A. Arain, D. Feldbaum, V. V. Frolov, M. Heintze, D. Hoak, E. A. Khazanov, A. Lucianetti, R. M. Martin, G. Mueller, O. Palashov, V. Quetschke, D. H. Reitze, R. L. Savage, D. B. Tanner, L. F. Williams, and W. Wu, "Thermal effects in the input optics of the enhanced laser interferometer gravitational-wave observatory interferometers," Rev. Sci. Instrum. **83**, 033109 (2012).

17. *New Focus 1611 Photodetector* (2011). http://assets.newport.com/webDocuments-EN/images/15178.pdf.

18. *Raicol RTP Specifications* (2006). http://www.optoscience.com/maker/raicol/pdf/catalog%20raicol_screen.pdf.

19. J. J. Carvajal, P. Segonds, A. Peña, J. Zaccaro, B. Boulanger, F. Díaz, and M. Aguiló, "Structural and optical properties of RbTiOPO$_4$: Nb crystals," J. Phys.: Condens. Matter **19**, 116214 (2007).

20. O. Gobert, N. Fedorov, G. Mennerat, D. Lupinski, D. Guillaumet, M. Perdrix, A. Bourgeade, and M. Comte, "Wavelength dispersion measurement of electro-optic coefficients in the range of 520 to 930 nm in rubidium titanyl phosphate using spectral interferometry," Appl. Opt. **51**, 594–599 (2012).

21. K. Somiya, Y. Chen, S. Kawamura, and N. Mio, "Frequency noise and intensity noise of next-generation gravitational-wave detectors with RF/DC readout schemes," Phys. Rev. D **73**, 122005 (2006).

1. Introduction

The advanced Laser Interferometer Gravitational-Wave Observatory (aLIGO) consists of two detectors located in Hanford, WA and Livingston, LA. These 4 km long Michelson interferometers are built to detect gravitational waves in the 10 Hz to 10 kHz frequency band [1, 2]. Initial LIGO set multiple important limits on the generation of gravitational waves [3–5]. Upgrades to the interferometers, which are currently nearing completion, are expected to yield the first detections within the next few years [6]. A basic sketch of the upgraded aLIGO interferometer design is shown in Fig. 1. The interferometer's mirrors act as test masses, experiencing a length displacement resulting from the strain of a passing gravitational wave. The gravitational wave signal is read out as the differential arm length changes (DARM) in the interferometer. This signal is enhanced by using Fabry-Perot resonant cavities as the interferometer's arms. In addition to the arm cavities (which are formed by the input test mass (ITM) and end test mass (ETM) mirrors) LIGO also uses a power recycling mirror (PRM) to increase the power circulating in the arm cavities; furthermore, aLIGO adds a signal recycling mirror (SRM) to form the signal recycling cavity, which adds the ability to tune the frequency response of the detector [7].

For aLIGO to operate, the laser must remain on resonance with the two arm cavities as well as the power recycling cavity. Several longitudinal degrees of freedom need to be controlled to keep the interferometer at this operating point. The aLIGO interferometer uses a phase modulation/demodulation scheme [8–10] to produce the necessary control signals for feedback. Two sets of radio frequency sidebands are imprinted on the carrier by phase modulation in an electro-optic modulator (EOM). Beat signals, produced by the interaction of the phase-modulated light with the interferometer, are detected and demodulated at various points in the interferometer (see eg. POP and REFL in Fig. 1) to create the error signals for feedback.

A scheme for producing two sets of frequency sidebands by phase modulating the laser field in the two arms of a Mach-Zehnder (MZ) interferometer has been explored [11], along with the effect of carrier-sideband relative phase noise (due to MZ arm length noise) on a LIGO heterodyne RF-readout scheme. The aLIGO detectors use a homodyne (DC) readout of DARM, which is less susceptible to carrier-sideband phase noise, but still has a requirement on laser power noise which couples into detector strain noise via radiation pressure noise. This paper discusses a novel method for stabilizing MZ arm lengths in a parallel phase modulation scheme as well the effect of MZ differential arm length noise on laser power noise in the context of the requirements in aLIGO.
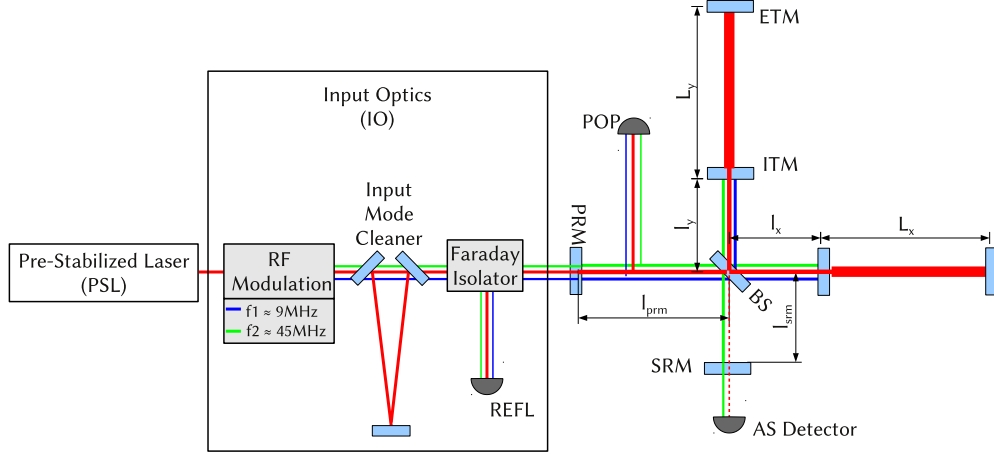

Fig. 1. The aLIGO interferometer is composed of the Fabry-Perot arm cavities as well as the power-recycling and the signal-recycling cavity. Three of the photodetector output ports are labeled: The reflected light pickoff (REFL), the power recycling cavity pickoff (POP), and the interferometer's anti-symetric port (AS). The carrier (red) and two sidebands (blue and green) are designed to be resonant in different parts of the interferometer.

2. Background

Radio frequency sidebands are imprinted onto the laser carrier by phase modulation in the 'RF Modulation' portion of the Input Optics shown in Fig. 1. The sidebands are created in an Electro-Optic Modulator (EOM) by passing the laser light through an electro-optic crystal and applying a time varying electric field (with voltage $V_1 \sin(\Omega_1 t)$) across the crystal (of thickness d). The modulated laser field exiting the EOM, E_{mod1}, is the result of the incident laser field ($E_{\mathrm{inc}} = E_0 e^{i\omega_0 t}$) gaining a time-dependent phase term ($m_1 \sin(\Omega_1 t)$), with a modulation depth (m_1) proportional to the field applied across the crystal and the crystal's electro-optic coefficient (r). The phase modulated laser field can be expanded in terms of Bessel functions, J_n, using the Jacobi-Anger expansion. This shows that for small modulation depths the modulated light is composed of three frequency components: the carrier and the two sidebands that are offset from the carrier frequency by the modulation frequency, $\pm f_1 = \pm \Omega_1/2\pi$. The amplitude of the field components are proportional to the Bessel functions of the modulation depth:

$$E_{\mathrm{mod1}} = E_0 e^{i[\omega_0 t + m_1 \sin(\Omega_1 t)]} = E_0 e^{i\omega_0 t} \sum_{\ell=-\infty}^{+\infty} J_\ell(m_1) e^{i\ell(\Omega_1 t)}$$

$$\approx E_0 [J_0(m_1) e^{i\omega_0 t} + J_1(m_1) e^{i(\omega_0 + \Omega_1)t} - J_1(m_1) e^{i(\omega_0 - \Omega_1)t}] \tag{1}$$

An illustration of the carrier and sideband spectrum is shown in Fig. 2(a).

2.1. Phase modulation in aLIGO

The aLIGO interferometer has five main longitudinal degrees of freedom to control [10]. These degrees of freedom (DOFs) are: the differential motion of the interferometer's arms (DARM), the common motion of the arms (CARM), the length of the short Michelson (MICH), the length of the power recycling cavity (PRCL), and the length of the signal recycling cavity (SRCL). The DOFs are outlined in Table 1.

Relative length information for controlling the optics' positions is contained in the beats between the different frequency components of the laser. The length error signals for each degree of freedom are formed by demodulating the laser at one of the photodetector ports with the appropriate frequency. In order to produce the error signals necessary to control these degrees of freedom two sets of frequency sidebands are added to the carrier at $f_1 \approx 9\,$MHz and $f_2 = 5f_1 \approx 45\,$MHz. These sideband frequencies were chosen, along with the lengths of the Signal Recycling Cavity (SRC) and Power Recycling Cavity (PRC), to allow both frequencies to be resonant in the PRC, but with only f_2 resonant in the SRC. The carrier alone is resonant in the two arm cavites (Fig. 1). The arm cavity degrees of freedom are formed by the beat between the carrier and itself for DARM and the demodulation of the beat between the carrier and a sideband (Ω_1) to produce the CARM error signal. The error signals for the non-arm-cavity degrees of freedom (MICH, SRCL, PRCL) need to be independent of the Fabry-Perot arm lengths. Originally, to produce these non-arm-cavity length signals a double demodulation scheme was proposed. Under this scheme the non-arm-cavity length signals would have been read from the beat between the two sidebands instead of between the carrier and a sideband [12]. The outline of this previous demodulation scheme is given in Table 1.

Table 1. Summary of the major DOFs in the aLIGO interferometer along with a previous demodulation scheme for error signal formation. Lengths and ports are defined in Fig. 1.

DOF	Length Definition	Sensing Port	Demod Freq
DARM	$L_x - L_y$	AS	DC
CARM	$L_x + L_y$	REFL	Ω_1
MICH	$l_x - l_y$	AS	$\Omega_1 \otimes \Omega_2$
PRCL	$l_{prm} + \frac{l_x + l_y}{2}$	REFL	$\Omega_1 \otimes \Omega_2$
SRCL	$l_{srm} + \frac{l_x + l_y}{2}$	POP	$\Omega_1 \otimes \Omega_2$

2.1.1. Modulation in series

The baseline design for aLIGO phase modulation is to produce multiple sidebands by modulating the laser in series [13]. A second EOM (driven by $V_2 \sin \Omega_2 t$) modulates the output of the first EOM, E_{mod1}, given in Eq. (1). This AC voltage causes the laser to pick up a second time dependent phase term ($m_2 \sin \Omega_2 t$) which mixes with the first to give the laser field E_{mod2}:

$$
\begin{aligned}
E_{mod2} = E_{mod1} & e^{im_2 \sin \Omega_2 t} \\
\approx E_0 [& J_0(m_1)J_0(m_2)e^{i\omega_0 t} + J_0(m_1)J_1(m_2)e^{i(\omega_0+\Omega_2)t} - J_0(m_1)J_1(m_2)e^{i(\omega_0-\Omega_2)t} \\
& + J_1(m_1)J_0(m_2)e^{i(\omega_0+\Omega_1)t} - J_1(m_1)J_0(m_2)e^{i(\omega_0-\Omega_1)t} + J_1(m_1)J_1(m_2)e^{i(\omega_0+\Omega_1+\Omega_2)t} \\
& - J_1(m_1)J_1(m_2)e^{i(\omega_0+\Omega_1-\Omega_2)t} - J_1(m_1)J_1(m_2)e^{i(\omega_0-\Omega_1+\Omega_2)t} + J_1(m_1)J_1(m_2)e^{i(\omega_0-\Omega_1-\Omega_2)t}]
\end{aligned}
\tag{2}
$$

where other terms of similar magnitude to $J_1 J_1$ (ie $J_0 J_2$) are omitted for brevity. Equation (2) shows the first pair of frequency sidebands are offset from the carrier by Ω_1 and have an am-
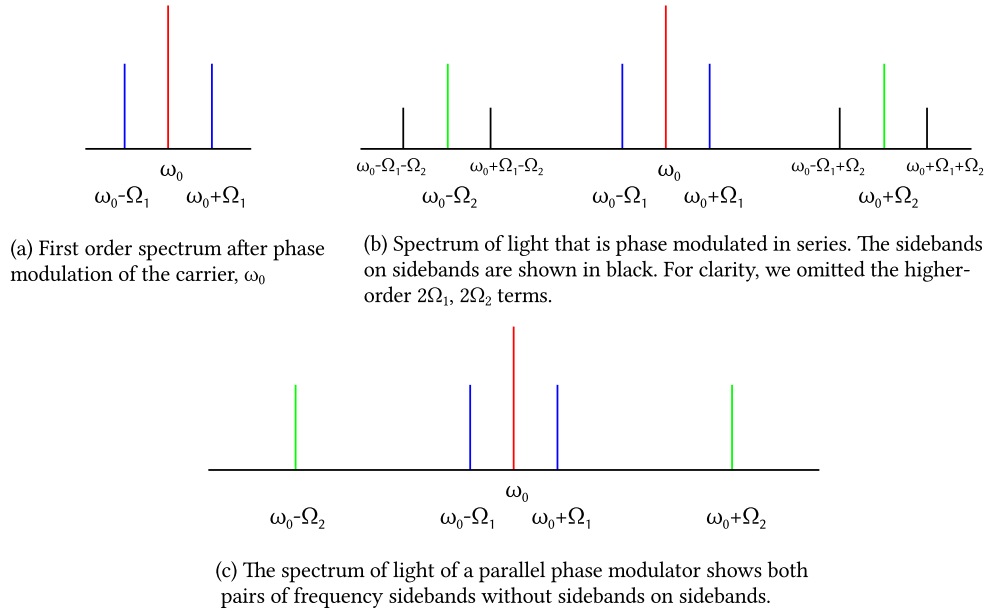
(a) First order spectrum after phase modulation of the carrier, ω_0

(b) Spectrum of light that is phase modulated in series. The sidebands on sidebands are shown in black. For clarity, we omitted the higher-order $2\Omega_1$, $2\Omega_2$ terms.

(c) The spectrum of light of a parallel phase modulator shows both pairs of frequency sidebands without sidebands on sidebands.

Fig. 2. Illustrations of the spectra of light produced by three different modulation schemes.

plitude proportional to $J_1(m_1)J_0(m_2)$; likewise, the second pair of sidebands are proportional to $J_0(m_1)J_1(m_2)$. The mixed sidebands, the terms proportional to $J_1(m_1)J_1(m_2)$, are termed "sidebands on sidebands". The spectrum of light modulated in series is illustrated in Fig. 2(b).

A problem arises when series phase modulation is used in a double demodulation scheme due to these sidebands on sidebands producing extraneous length signals of the same order as the length signals desired for feedback [11]. Double demodulation retrieves length information stored in the beat between the two sidebands by demodulating first with one and then with the second sideband frequency, effectively demodulating at the sum and difference frequency of the two sidebands. This produces an error signal whose amplitude is proportional to the product of the amplitudes of the two sidebands: $err_{s_1 \times s_2} \propto J_1(m_1)J_0(m_2) \times J_0(m_1)J_1(m_2)$. When using series modulation, sidebands on sidebands are created and exist at the same sum/difference frequencies. These sidebands on sidebands beat with the carrier, whose phase information depends on the two arm-cavity DOFs (DARM and CARM). Double demodulation will include this beat and will produce a term that is proportional to the product of the carrier and sidebands on sidebands: $err_{\text{carrier} \times \text{sos}} \propto J_0(m_1)J_0(m_2) \times J_1(m_1)J_1(m_2)$. Because the unwanted carrier/sideband-on-sideband term is of the same order as the beat between the sidebands it can be difficult to separate the non-arm-cavity degrees of freedom from the CARM and DARM degrees of freedom; this difficulty was observed at the LIGO 40m prototype at Caltech and is shown in the large off-diagonal terms of the signal matrix derived from optical simulation in [12]. The modern baseline length sensing and control scheme does not use double demodulation to form sensing signals for MICH or PRCL. It does demodulate the REFL signal with $f_2 \mp f_1$ frequencies for the formation of the SRCL error signals, however, the off-diagonal terms from sidebands on sidebands in the modeled sensing matrices are small and not expected to be problematic [10]. As a risk reduction experiment, a parallel phase modulator creates two sets of frequency sidebands without sidebands on sidebands.

2.1.2. Modulation in parallel

Sidebands on sidebands can be avoided using an interferometric parallel phase modulation scheme [12]. An example setup is shown in Fig. 3. The incoming beam is split and modulated in both arms separately. The beams from the x and y arms being recombined at the beam splitter are described as:

$$E_{\text{x,y}} = \frac{E_0}{\sqrt{2}} e^{-i(\omega_0 t + m_j sin\Omega_j t + \phi_{Lj})}, \qquad j = 1, 2 \tag{3}$$

where ω_0 is the laser carrier frequency, m_j is the modulation depth, Ω_j is the modulation frequency applied in EOM_j, and ϕ_{Lj} is the phase gained by the beam traversing its respective arm. The beams are then recombined at the beam splitter. The field leaving the interferometer's bright port (BP) is given by:

$$
\begin{aligned}
E_{\text{BP}} &= E_{\text{x}} + E_{\text{y}} \\
&\approx \frac{E_0}{2} e^{-i\phi_{L1}} [J_0(m_1) e^{-i\omega_0 t} + J_1(m_1) e^{-i(\omega_0 + \Omega_1)t} - J_1(m_1) e^{-i(\omega_0 - \Omega_1)t}] \\
&\quad + \frac{E_0}{2} e^{-i\phi_{L2}} [J_0(m_2) e^{-i\omega_0 t} + J_1(m_2) e^{-i(\omega_0 + \Omega_2)t} - J_1(m_2) e^{-i(\omega_0 - \Omega_2)t}]
\end{aligned}
\tag{4}
$$

The bright port of the interferometer contains the carrier and two sets of sidebands without sidebands on sidebands, its spectrum is shown in Fig. 2(c). Parallel phase modulation has been tested [14] and implemented in the LIGO 40 m prototype [15] using a PZT actuated mirror for feedback to control the Mach-Zehnder's arm lengths. PZT actuation limited the bandwidth in the feedback loop, limiting the suppression of differential arm length noise. This paper explores a setup which uses the modulator's RTP electro-optic crystals for phase correction allowing for much greater bandwidth and actuation of the MZ arm lengths at higher frequencies.
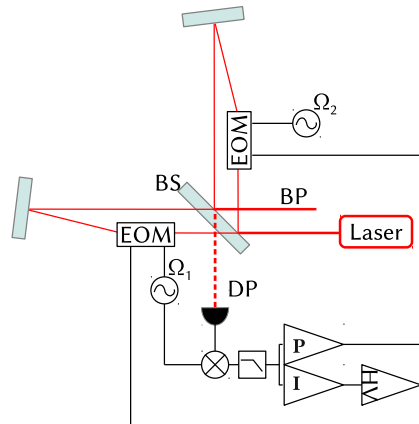

Fig. 3. The Mach-Zehnder experimental setup.

3. Mach-Zehnder experimental implementation

A parallel phase modulation scheme would mean adding a new optical system and control loop to the very sensitive aLIGO interferometers. It is thus a fruitful endeavor to have a parallel phase modulation scheme designed and characterized to meet aLIGO power noise requirements so, should the need arise, it could be implemented without adding excessive noise to the aLIGO

detectors. The interferometric experimental setup is shown in Fig. 3 and pictured in Fig. 4. The setup uses a $\lambda = 1064$ nm wavelength laser which is split at the beam splitter (BS); in the first trip down each arm the field is modulated in a $2.85°$ dual-wedged RTP electro-optic crystal measuring 4 mm $\times$ 4 mm $\times$ 40 mm ($W \times H \times L$), similar to the one used in initial LIGO and aLIGO [16]. Each crystal is mounted as an electro-optic modulator (EOM) including an RLC resonant circuit which applies a voltage across the crystal via a pair of 30 mm long electrodes. The x-arm is modulated at $f_1 = \frac{\Omega_1}{2\pi} = 48.575$ MHz, with a modulation depth of $m_1 = 0.14$, and the y-arm is modulated at $f_2 = 9.646$ MHz and $m_2 = 0.12$. The beam is then reflected and restraightend by the end mirrors; the return path is entirely through free space.
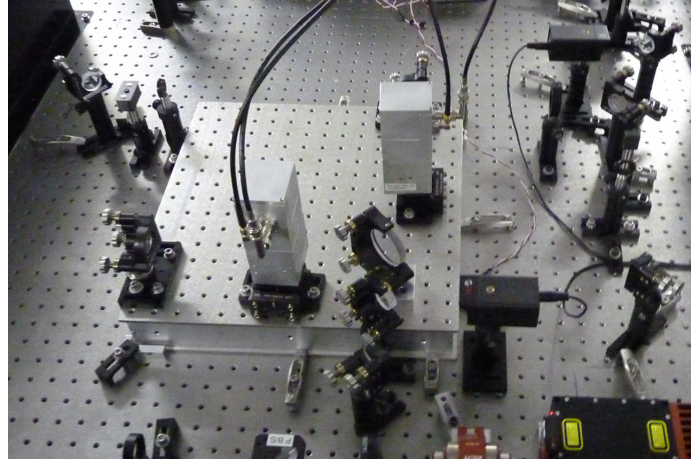

Fig. 4. A photograph of the Mach-Zehnder parallel phase modulator.

Differential arm length changes in the Mach-Zehnder (MZ) interferometer produce intensity noise in both beams exiting the interferometer and will need to be controlled. To measure differential arm length noise, and subsequently apply the necessary feedback, a linearized error signal is needed. The error signal is formed by demodulating the light at the Mach-Zehnder's dark port with the x-arm's modulation frequency ($f_1 = 48.575$ MHz). A photodetector (New Focus 1611 [17]) is used to readout the laser field at the bright port as well as the dark port, whose field is the same as the bright port's (Eq. (4)), but with an additional π phase shift in the x-arm. The photodetector produces a voltage according to its transimpedance gain (G_{TI}), responsivity (R_{PD}), and the intensity at the dark port (DP):

$$
\begin{aligned}
V_{DP} &= G_{TI} \times R_{PD} \times |E_{DP}|^2 \\
&\approx G_{TI} R_{PD} \times |\frac{E_0}{2} e^{-i(\phi_{L1}+\pi)} [J_0(m_1)e^{-i\omega_0 t} + J_1(m_1)e^{-i(\omega_0+\Omega_1)t} - J_1(m_1)e^{-i(\omega_0-\Omega_1)t}] \\
&\quad + \frac{E_0}{2} e^{-i\phi_{L2}} [J_0(m_2)e^{-i\omega_0 t} + J_1(m_2)e^{-i(\omega_0+\Omega_2)t} - J_1(m_2)e^{-i(\omega_0-\Omega_2)t}]|^2
\end{aligned}
\tag{5}
$$

Because the error signal is being formed with the Ω_1 modulation frequency, the Ω_2 terms will

not show up after mixing and filtering so we can ignore the Ω_2 terms:

$$V_{DP} = G_{TI}R_{PD}\frac{P_0}{4}\{2 + J_0(m_1)[e^{-i(\phi_{L1}-\phi_{L2}+\pi)} + e^{i(\phi_{L1}-\phi_{L2}+\pi)}]$$
$$+ 2J_1(m_1)\sin(\Omega_1 t)[e^{i(\phi_{L1}-\phi_{L2}+\pi)} - e^{-i(\phi_{L1}-\phi_{L2}+\pi)}]\}$$

$$V_{DP} = G_{TI}R_{PD}\frac{P_0}{2}\{1 + J_0(m_1)\cos(\Delta\phi + \pi) - 2J_1(m_1)\sin(\Omega_1 t)\sin(\Delta\phi)\} \tag{6}$$

where P_0 is the laser power entering the interferometer and $\Delta\phi = \phi_{L1} - \phi_{L2}$ is the phase difference between the recombined beams. The error signal is formed by demodulating and filtering the dark port signal with the original modulation signal, $\sin(\Omega_1 t + \phi_{EO})$, where ϕ_{EO} is demodulation phase difference. This gives the error signal:

$$V_{err} = \frac{P_0}{2}G_{TI}R_{PD}J_1(m_1)\cos(\phi_{EO})\sin(\Delta\phi) \tag{7}$$

The demodulation phase ϕ_{EO} can easily be zeroed, by either adding appropriate length of cable or using a phase shifter, maximizing the error signal slope. The error signal is a sine function of the path length difference between the two arms and has the needed zero crossing and linearity at the dark fringe to be an effective feedback control signal. This error signal has the advantage of an infinite locking range, allowing the arm length difference to be pushed to zero starting from any microscopic path length difference, but the disadvantage of having a relatively small error signal slope compared to other demodulation techniques, such as finesse enhanced Fabry-Perot cavity phase demodulation. A similar signal can be derived at the bright port.
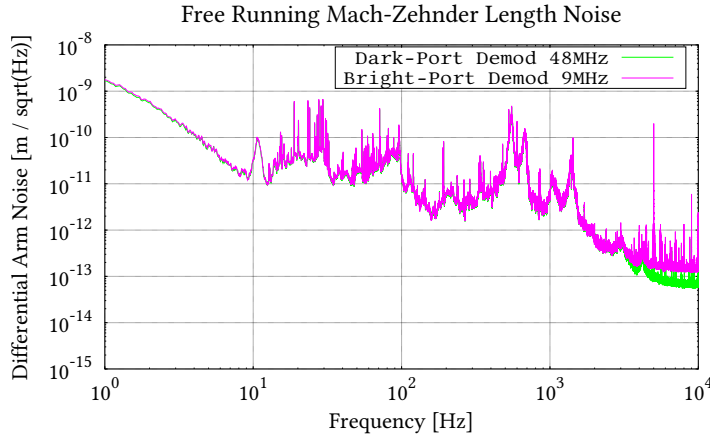

Fig. 5. Differential arm noise of the free-running Mach-Zehnder measured by demodulating the bright and dark ports (purple and green) at 48.575 and 9.646 MHz respectively.

The linear portion of the dark and bright-port demodulated error signals were independently calibrated then simultaneously measured in time; computing the power spectral density of these length fluctuations reveals the frequency components of the free-running Mach-Zehnder's differential arm length changes in open air (Fig. 5). The agreement between the dark and bright port demodulated signals indicate the error signals are dominated by the actual length noise signal and that the error signals are well calibrated.

The electro-optic crystals used for modulation are also used as length actuators in the arm length feedback system. Applying the control signal's voltage across the crystal changes its

index of refraction. This adjusts the arm's optical path length, compensating for the arm length changes. We used Rubidium Titanyl Phosphate (RTP) crystals obtained from Raicol [18], with the same dimensions and material as the electro-optic crystals used in aLIGO. The Sellmeier coefficients for the index of refraction have been measured for RTP [19] to give an index of refraction $n_{0z} = 1.8580$ at 1064 nm. The electro-optic coefficient r_{33} has been measured in the range from 520 to 930 nm [20]; using these fitted Sellmeier coefficients gives an EO coefficient of $r_{33} = 34.35 \frac{\text{pm}}{\text{V}}$ at 1064 nm.

In order to make use of the largest electro-optic coefficient, r_{33}, the laser propagates through the crystal with polarization in the z-direction (p-polarization) and has the external driving electric field in the z-direction (E_z). It is convenient to describe the response of EO crystals in terms of the voltage required to produce an optical path length change of $\frac{\lambda}{2}$ or π radians:

$$V_\pi = \frac{\lambda d}{n_{0z}^3 r_{33} L} \tag{8}$$

where d = 4 mm is the crystal thickness and L = 30 mm is the length of the electrodes applying the field across the crystal. We measured the response of the crystals by driving the crystals with a triangular wave with an amplitude of $A = 2$ kV and frequency of f_d, producing fringes at a rate of $f_f = f_d \frac{2A}{V_\pi}$ and monitoring the fringes by DC readout of the Mach-Zehnder. This produced a measured response in the aLIGO frequency band of $V_\pi \approx 660$ V for one crystal, or ≈ 330 V for two crystals in a push-pull configuration. We observed a yet unexplained 10% decrease in the responsivity of the crystals when driven below 1 Hz.

The control signal to be applied across the crystal is formed by amplifying and filtering the error signal with a custom proportional-integral (PI) servo. In order to provide the higher voltage needed for the necessary feedback range, the low frequency integral part of the control signal is amplified with a Trek 2220 high-voltage amplifier before being applied to the y-arm crystal. The proportional signal is sent directly from the custom servo to the x-arm crystal, providing the high frequency response. The cross-over frequency between the I and P parts is at 230 Hz and the unity gain crossing is at 200 kHz.
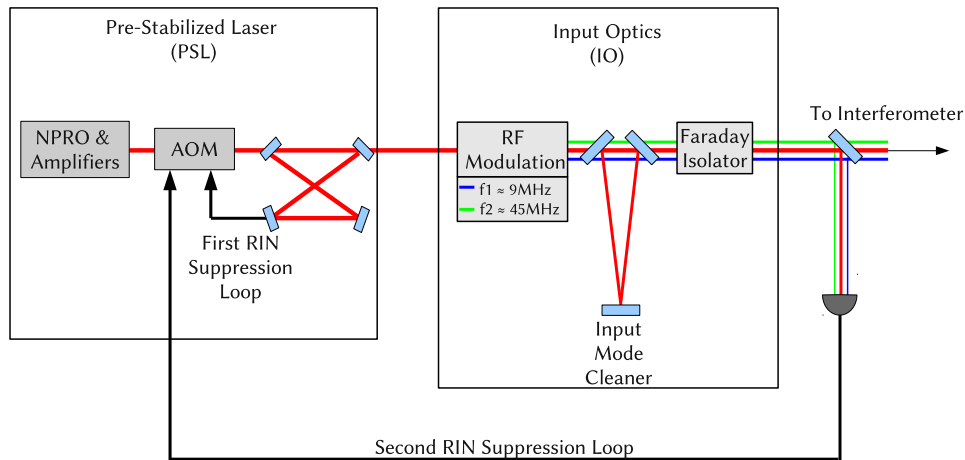

Fig. 6. The locations of the power stabilization pickoffs. The RF modulation is inside the second feedback loop.
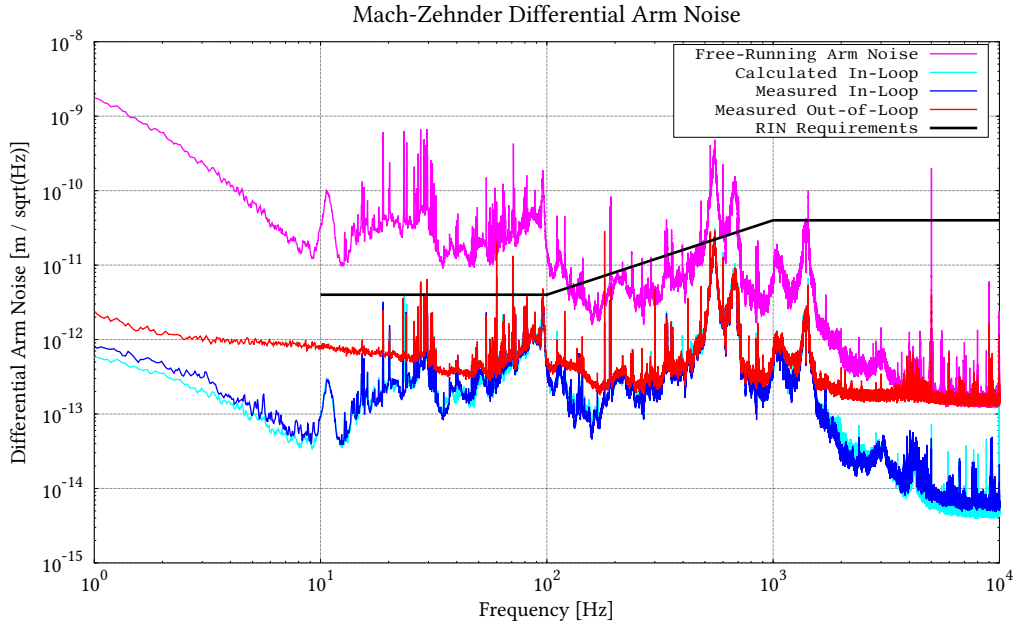
Fig. 7. The Mach-Zehnder's measured closed-loop differential arm noise (In-loop (Blue) and Out-of-loop (Red)). The calculated level of suppressed noise (Cyan) is based on the feedback and the free-running noise (Magenta). The requirement for aLIGO, based on the equivalent RIN produced from MZ differential arm motion, is shown in Black.

4. Results and conclusion

Feedback is necessary to stabilize the Mach-Zehnder's arm lengths and reduce fluctuations in the laser power leaving the interferometer. The transfer function of aLIGO's laser's relative intensity noise (RIN) to aLIGO's strain sensitivity shows that laser power noise couples to strain noise at low frequencies mostly through radiation pressure imbalance in the two arms [21]. LIGO's technical noise requirement (that no technical noise source should produce more than 10% of the aLIGO design strain noise) puts a noise limitation on the RIN of the laser entering the aLIGO interferometer of $2 \times 10^{-9}\,\mathrm{Hz}^{-1/2}$ at 10 Hz.

The power stabilization in aLIGO consists of two feedback loops, shown in Fig. 6. The first loop reduces power noise down to $2 \times 10^{-8}\,\mathrm{Hz}^{-1/2}$ at 10 Hz, and a second feedback loop will reduce it further to the interferometer's requirement. LIGO's RF modulation lies after the first power stabilization loop, but inside the second power stabilization loop. The goal of the Mach-Zehnder's arm length stabilization is to reduce length noise such that intensity noise in the LIGO band due to the Mach-Zehnder's arm length noise is not a burden on the second power stabilization loop. The power exiting the Mach-Zehnder interferometer as a function of its differential arm length, ΔL, is:

$$P(\Delta L) = \frac{P_0}{2}[1 + \cos(\frac{2\pi}{\lambda}\Delta L)] \qquad (9)$$

To calculate the RIN due to Mach-Zehnder arm length noise, δL, we expand this about the differential arm locking point, L_{RMS}, which gives

$$RIN = \frac{2\pi^2}{\lambda^2}L_{RMS}\delta L \qquad (10)$$

where L_{RMS}, the rms distance of the locking point from the dark fringe, is due to the unavoidable (but suppressed) RMS of the differential arm noise as well as any possible unwanted electronic offset. L_{RMS} was measured to be 0.3 nm, giving the RIN equivalent length noise requirement seen in Fig. 7.

The closed loop differential arm noise was measured by recording the in-loop and out-of-loop length error signals. Figure 7 shows that the linear spectral density of the in-loop error signal (blue) is reduced to the level calculated (cyan), based on the free-running length noise (magenta) and the feedback components' transfer functions. The actual differential arm length noise is best seen in the out-of-loop noise spectrum (red). This meets, by a factor of 5 at low frequencies and 30 at high frequencies, the arm length stability requirements (black) to not induce excessive power fluctuations in the laser carrier entering the gravitational wave detector interferometer.

Mechanical resonances of the optics can be seen as peaks in the hundred hertz through kilo-hertz range, most notably the lines at 680 and 550 Hz corresponding to the resonance of x and y end mirrors of the Mach-Zehnder. These are excited acoustically and scale with this environmental noise. The feedback servo was designed specifically to bring these peaks down to the requirement level, and in the unlikely case the environment is noisier at the gravitational-wave detector more gain can be added in the Mach-Zehnder feedback loop. The gain at these higher frequencies is enabled by this setup's use of the electro-optic crystals as high-speed length actuators. This allowed us to achieve a unity gain frequency of 200 kHz, an order of magnitude higher than the PZT actuated parallel modulation scheme [11]. The level of noise suppression through the entire aLIGO band makes this setup a tested and viable solution for creating multiple RF sidebands without sidebands on sidebands, should the need arise.

Acknowledgments